Study of the Air-Sea Interaction During Typhoon Kaemi (2006)*

LIU Lei[1†](刘 磊), FEI Jianfang[1](费建芳), LIN Xiaopei[2](林霄沛), SONG Xiangzhou[2,3](宋翔州), HUANG Xiaogang[1](黄小刚), and Cheng Xiaoping[1](程小平)

1 *Institute of Meteorology, PLA University of Science and Technology, Nanjing* 211101*, China*

2 *College of Physical and Environmental Oceanography, Ocean University of China, Qingdao* 266100*, China*

3 *Department of Physical Oceanography, Woods Hole Oceanographic Institution, Woods Hole, Massachusetts* 02543*, USA*

(Received August 24, 2010; in final form April 1, 2011)

ABSTRACT

The high-resolution Weather Research and Forecasting (WRF) model is coupled to the Princeton Ocean Model (POM) to investigate the effect of air-sea interaction during Typhoon Kaemi that formed in the Northwest Pacific at 0000 UTC 19 July 2006. The coupled model can reasonably reproduce the major features of ocean response to the moving tropical cyclone (TC) forcing, including the deepening of ocean mixed layer (ML), cooling of sea surface temperature (SST), and decaying of typhoon.

Due to the appearance of maximum SST cooling to the left of the simulated typhoon track, two points respectively located to the left (16.25°N, 130.1°E, named as A, the maximum SST cooling region) and right (17.79°N, 130.43°E, named as B) of the typhoon track are taken as the sampling points to study the mechanisms of SST cooling. The low temperature at point A has a good correlation with the 10-m winds but does not persist for a long time, which illustrates that the temperature dropping produced by upwelling is a quick process. Although the wind-current resonance causes oscillations to the left of typhoon track at point A, the fluctuation is not so strong as that at point B. The thin ML and upwelling produced by the Ekman pumping from strong 10-m winds are the main reason of maximum SST cooling appearing to the left of the typhoon track. Due to weaker 10-m winds and thicker and warmer ML at point B, the colder water under the thermocline is surpressed and the temperature dropping is not dramatic when the strongest 10-m winds occur. Afterwards, the temperature gradually decreases, which is found to be caused by the inertial oscillations of the wind-current system.

Key words: typhoon, coupled mesoscale atmosphere-ocean model, SST cooling, mixed layer, wind-current resonance

Citation: Liu Lei, Fei Jianfang, Lin Xiaopei, et al., 2011: Study of the air-sea interaction during Typhoon Kaemi (2006). *Acta Meteor. Sinica*, **25**(5), 625–638, doi: 10.1007/s13351-011-0507-8.

1. Introduction

The northwestern Pacific is the only region where tropical cyclones (TCs) originate all year round and a key region for generation and development of category five cyclones (typhoons) (Lin et al., 2008). Due to the limited open sea observations and the low temporal or spatial resolution of available data, the development of coupled air-sea models is necessary for the study of air-sea interaction under typhoon conditions. By coupling MM5 (the Fifth-Generation NCAR/Penn State Mesoscale Model), POM (Princeton Ocean Model), and WAM (Wave Analysis Model) models, Bao et al. (2000) studied the development of Hurricane Opal and found that the simulated hurricane intensity was sensitive to the ocean conditions. Black et al. (2007) used a three-way air-ocean-wave coupled system (MM5, 3DPWP (three-dimensional primitive equation hydrostatic upper-ocean model), and Wave Watch III) from the University of Miami (Chen et al., 2007) to provide field operation guidance. Recently, Chen et al. (2010) used a two-way air-sea coupled model to study the

*Supported by the China Meteorological Administration Special Public Welfare Research Fund for Meteorological Profession (GYHY201106004), National Natural Science Foundation of China (41005029), and Doctoral Students Visiting Program of the Chinese Ministry of Education.

†Corresponding author: Liu541226@sina.com.

air-sea interaction and its impact on two different weather scenarios. The first is Hurricane Katrina and the second is the effect of wind- and current-induced island wakes and their impact on the local electromagnetic (EM) and acoustic propagation characteristics in the southern California Bight region.

As the underlying surface, ocean is one of the essential factors affecting TC intensity and structure. A TC obtains its main energy from ocean, and its intensity is closely associated with the underlying sea surface temperature (SST) (Tuleya and Kurihara, 1982; Emanual, 1986). The warm ocean mixed layer (ML) provides necessary thermal energy and surface heat flux for the development of convection (Emanual, 1988; Gray, 1998). Raper (1992) analyzed both concurrent and preceding SST anomalies of local TC activities over the Atlantic and pointed out that TCs extracted energy from the warm tropical ocean, and then released heat into the upper tropospheric airflow which further fueled the storm's development. Emanuel (1988) treated TC as a Carnot engine and found that the SST cooling of 1.0°C can increase the TC central pressure by 10 hPa. Holland (1997) used a thermodynamic method and estimated a change of 33 hPa in the sea level pressure (SLP). Zhu et al. (2004) found that when SST decreased by 1.0°C, a TC would weaken by 20 hPa. Similar results were also shown by Chan et al. (2001) and Ren and William (2006).

A distinctive feature of the upper ocean response to a moving TC is the SST cooling. With winds rotating around the TC center, it produces a wind forcing that varies at a frequency close to the inertial frequency, given a correctly matched size and translation speed. The inertial motion and cooling in the upper ocean are enhanced during such wind-current resonant events (Crawford and Large, 1996).

In order to investigate the ocean response during typhoon passage in northwestern Pacific, we have developed a high-resolution mesoscale air-sea coupled model and simulated Typhoon Kaemi which originated in this region.

The coupled model and its component models are described and the experimental design are introduced in Section 2. A brief overview of the evolution of Typhoon Kaemi is also presented. Section 3 validates the numerical simulations and describes the ocean response. In Section 4, the thermodynamic and dynamic mechanisms of air-sea interaction affecting the ocean response are investigated. A summary is given in Section 5.

2. Model description

2.1 Coupling strategy

The shared memory and semaphores of interprocess communication under the Linux operation system are used as the pipe to transfer the data between two component models. The atmospheric model transfers longwave and shortwave radiation fluxes, sensible and latent heat fluxes, and 10-m winds to the ocean model, while the ocean model supplies SST to the atmospheric model. The two models exchange data per hour, which is reasonable in the study of ocean response, since the ocean response time is much longer than 1 h. The coupled model is integrated for 72 h, from 0000 UTC 20 to 0000 UTC 23 July 2006, during which Typhoon Keami was generated and experiencing a steady development. The atmospheric model output is saved every 6 h, and the oceanic model output is saved per hour in order to resolve the ocean internal structure.

2.2 Atmospheric model

The Weather Research and Forecasting (WRF) model version 3.1.1 is used as the atmospheric model. It is fully compressible and non-hydrostatic. The control equations are expressed in the flux form. The model employs the Arakawa C grid, which is advantageous in the high-resolution numerical simulation (Skamarock et al., 2005). Plenty of numerical experiments have been performed to investigate the TC structure with the WRF model. Gentry (2007) simulated a TC and studied how the TC intensity and structure were affected by changes in the horizontal grid spacing from 12 to 1 km. The inner core of a TC has also been simulated based on the WRF model (Corbosiero, 2007; Davis et al., 2007).

A bogus typhoon scheme in the WRF is utilized and the initial typhoon is close to the observation with the central SLP of 990 hPa. Details about the bogus typhoon scheme are available at http://www.mmm.ucar.edu/wrf/users/. The atmospheric model has a 15-km horizontal grid spacing and 27 vertical half-sigma layers. The domain is centered at 15.2°N, 130.5°E, and the time step of the integration is 60 s. Cloud processes are represented by the Kain-Fritsch parameterization scheme and surface processes are represented by the Monin-Obukhov parameterization scheme.

2.3 Ocean model

POM is used as the oceanic component in the coupled system. Details about this model can be found in the POM users guide (Mellor, 2004). Previous studies indicated that the POM could well reproduce the features of ocean. Kagimoto and Yamagate (1997) utilized the POM and successfully simulated the variations of seasonal transport of the Kuroshio. Xia et al. (2006) simulated the Yellow Sea with an improved version of POM and found two cold eddies.

The domain covers 5.75°–24.5°N, 120.75°–140.25°E, which is slightly larger than the domain of the atmospheric model. The horizontal grids are 118×113, with a resolution of 1/6°×1/6°. The vertical coordinates involve 16 sigma layers, with the maximum ocean depth of 3000 m. The region of the Philippine Islands is treated as a whole continent. The south of Taiwan Island in the northwestern corner of the model domain and the Philippine Islands are taken as the fixed boundary conditions. For example, the normal velocity perpendicular to shore is zero ($\boldsymbol{U} \cdot \boldsymbol{n}$=0). Since the region focused is relatively small and the open boundary is too wide, the open boundary condition has a direct impact on the simulation results. Thus, the 10-yr climatological data from the northwestern Pacific regional ocean model (Ma et al., 2009) are used as the open condition and the initial fields of water elevation and flow. The open boundary condition and initial field of thermohaline use the monthly-averaged Simple Ocean Data Assimiation (SODA) data. The open boundary condition of flow is defined by the first condition. The inflow of thermohaline applies the first condition, and the outflow uses the radiation condition. The sea surface wind stress is calculated from the 2005 three-day averaged Quick Scaterometer (QuikSCAT) data. The sea surface heat forcing assimilates the daily Advanced Microwave Scanning Radiometer (AMSR) SST data. The model is divided into the external and the internal mode. The time step for the external mode is 10 s while that for internal is 300 s. The model runs for 2 yr and gets a steady marine in 2005.

Based on the steady marine conditions, the climatological results of the regional ocean model (as mentioned above) are taken as the open boundary condition of water elevation and flow, and the monthly averaged SODA data are used as the open boundary condition of thermohaline. The sea surface wind stress is calculated from the 3-day averaged QuickSCAT data. The sea surface heat forcing uses the assimilated daily AMSR SST data. The ocean model runs untill 0000 UTC 20 July 2006 when typhoon occurred. Due to the lack of instantaneous observations of ocean current, the monthly averaged SODA data in July 2006 are utilized to validate the steady marine conditions. The comparison is shown in Fig. 1. The POM could correctly simulate the Kuroshio in the southeast of Taiwan Island, the Mindanao Cold Current in the southeast of the Mindanao Island, and the North Equatorial Countercurrent except for a deviation in the location of the North Equatorial Current. The simulated NEC is around 15°N while in SODA it is located around 9°–12°N.

2.4 Selected typhoon case

Typhoon Kaemi (2006) originated over the Northwest Pacific about 1600 km east of central Philippines in the afternoon of July 2006. It developed into an intense tropical storm on 20 July, then continually intensified into a typhoon, which finally landed in the coastal region of Taitung county of Taiwan Island at 1550 UTC 24 July. When the typhoon landed, the wind speed near its core was 40 m s^{-1}, and the maximum 10-m wind speed was more than 50 m s^{-1}. The typhoon passed Taiwan Island and entered the Taiwan Strait at 2000 UTC 24 July. Finally, it landed again in Jingjiang of Fujian Province, where the maximum wind speed was 33 m s^{-1}. Meanwhile, it

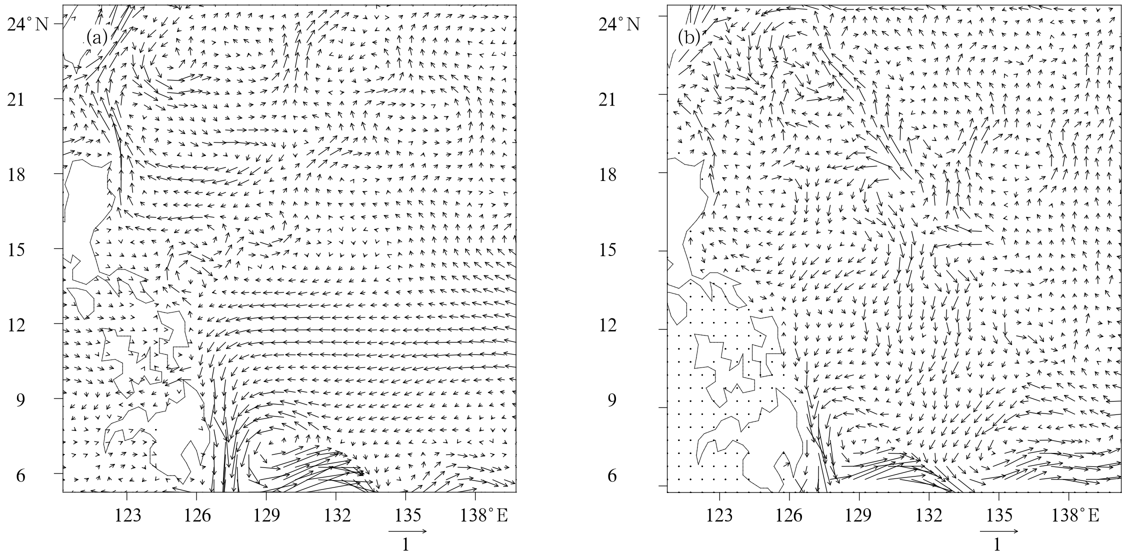

Fig. 1. Monthly averaged ocean current vectors from (a) the SODA observation and (b) the POM simulation in July 2006.

moved westward with the speed of 10–15 km h^{-1} and weakened into a tropical depression in Pinghe of Fujian Province at 2100 UTC 25 July. Then, it turned to north and slowed down, and moved to Jiangxi Province at noon of 26 July. At last, it disappeared in the central western Jiangxi in the afternoon of 26 July 2006.

2.5 Experimental design

Three numerical experiments are carried out and analyzed. The first experiment (CTRL) with the fixed-SST is designed to be an atmosphere–only case, which is run with the sole atmospheric model without the atmosphere-ocean coupling. In order to investigate the air-sea interaction, the second experiment (COUP) is designed to run with the coupled model. The third experiment (PTRL) is designed to run with merely the ocean model and the output is subtracted from COUP to study the SST anomaly, ocean ML depth (MLD), and ocean current distributions. The observation data of the intensity, track, and maximum wind of typhoon from the Shanghai Typhoon Institute, the TRMM satellite data, which have been widely used in the investigation of ocean response to typhoon (with focus on SST) (Jena et al., 2006; Yin et al., 2007; Wu et al., 2008), and the QuikSCAT (with focus on 10-m winds) are used to validate the numerical experimental results (CTRL and COUP).

3. Results

3.1 Simulated typhoon intensity and track

As shown in Fig. 2a, the simulated typhoons at the initial stage show a rapid intensification and reach the minimum center pressures of 952 and 957 hPa in CTRL and COUP at 42 h. The simulated intensifications are faster than the observed. The observed center pressure at the initial stage is gradually deepened and accelerated at 12 and 30 h. The pressure in COUP is closer to the observation before 42 h. The pressure bias at this period maybe results from the spin up associated with the bogus typhoon scheme. When the observed pressure remains constant from 42 to 72 h, the intensity of typhoon in COUP and CTRL exhibits a gradual decrease. Due to the SST cooling, the upward heat flux is prohibited, and the pressure anomalies in COUP are getting larger.

The simulated maximum 10-m winds shown in Fig. 2b are compared with the observation from the Shanghai Typhoon Institute from 12 to 72 h. The first 12-h results are excluded considering the model spin up problem. The simulated 10-m winds show gradual intensification from 12 to 24 h and a slight decrease during 24 to 30 h, followed by an increase till 48 h.

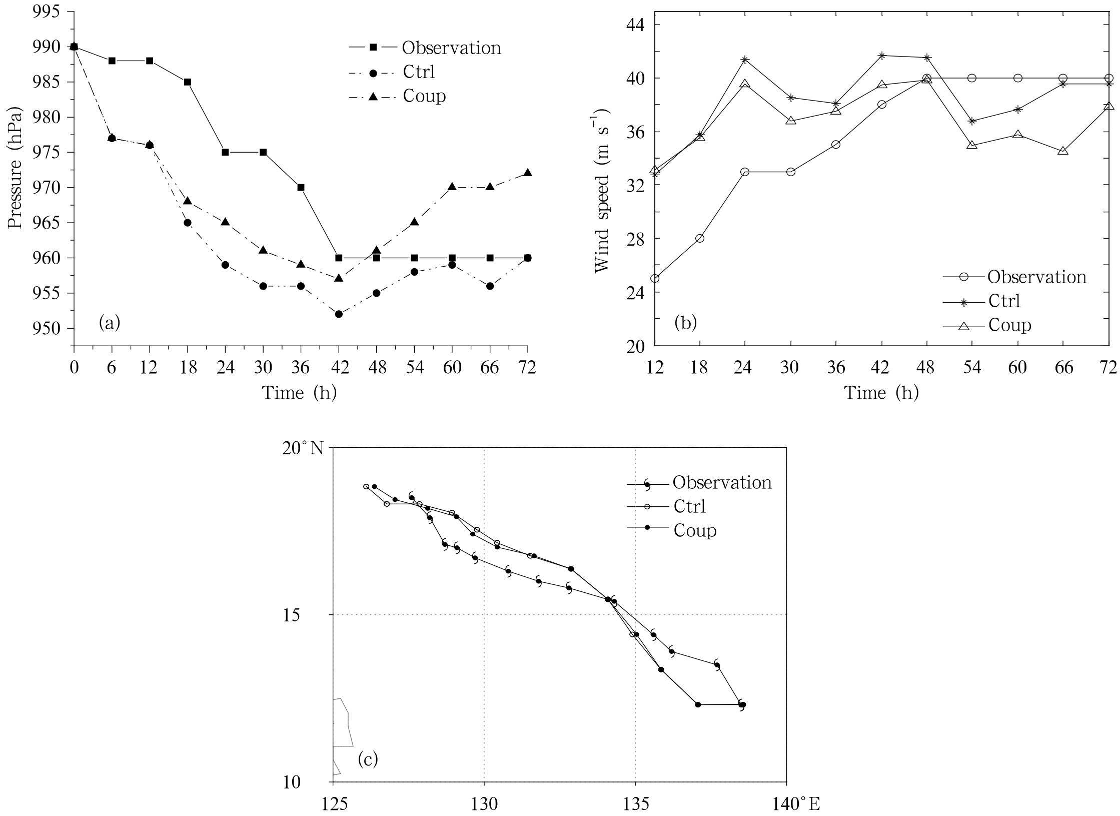

Fig. 2. (a) Minimum center pressure of typhoon, (b) maximum 10-m wind, and (c) the track of Typhoon Kaemi from observation, CTRL, and COUP.

Afterwards, the 10-m winds become weaker than the observation due to the decay of the simulated typhoon. Based on the above analysis, the simulated typhoon intensity change is generally in good agreement with the observation.

Previous studies obtained different results about whether the ocean response affects TC track. Using a TC model (a 8-layer ocean model coupled with the NOAA's GFDL atmospheric model), Bender et al. (1993) found that the westward track of the simulated typhoon gradually turned northward relative to the track in the fixed SST experiment, especially for the slow-moving storms. This track deviation was related to a systematic decrease in the azimuthally averaged tangential flow of the TC vortex. Huang et al. (2005) suggested that the SST cooling has an impact on the typhoon track, and the coupled model could reduce the error in the simulated TC track. However, Bender and Ginis (2000) and Zhu et al. (2004) indicated that the flow asymmetries induced by the ocean cooling are too small on scale to have significant effects on the typhoon track. In our experiments (Fig. 2c), as the bogus typhoon is included in the initial field, there is no error in the initial location of typhoon between the simulated and the observed. During the first 24 h, the simulated typhoon track in both CTRL and COUP exhibits a westward bias, while for the rest simulation time an eastward bias is found. The two numerical experiments get a very similar typhoon tracks compared to the observed best-track estimate. This suggests that the track simulation in this case is insensitive to the coupling process between the atmosphere and ocean.

3.2 Simulated SST, 10-m winds, and typhoon track

The SST, 10-m winds, and typhoon track from CTRL, COUP, and the observation during 42–66 h are shown in Fig. 3. The simulated SST in COUP is similar to the observation (Fig. 3e), both of which

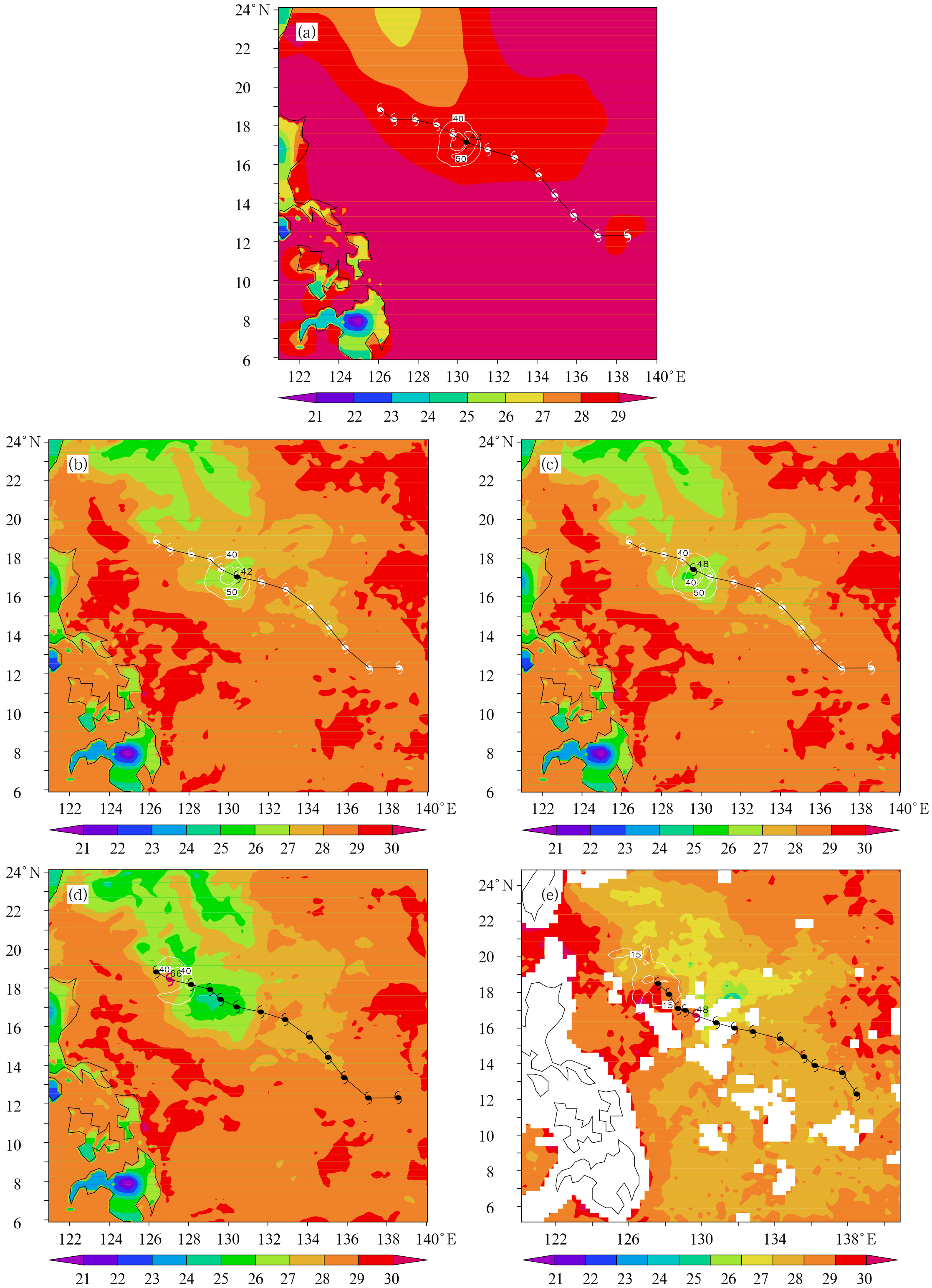

Fig. 3. SST (shading; unit: °C) and typhoon center from (a) CTRL at 42 h, (b, c, d) COUP at 42, 48, 66 h, respectively, overlapped with high speed winds (isograms; starting value: 40 m s^{-1}, interval: 10 m s^{-1}), and (e) the observation at 48 h, also superimposed with high speed winds near the typhoon center (isograms; starting value: 15 m s^{-1}, interval: 5 m s^{-1}).

display the same temperature of 28.5°C along the typhoon track and the lowest SST of 25.5°C near the typhoon center. Therefore, the coupled model can reasonably simulate the ocean response under the moving typhoon forcing. Due to the influence of typhoon cloud, there are some missing values near the typhoon center in the observation. The different sources of observation of the wind, SST, and typhoon track are not precisely consistent with each other. The 10-m winds in Fig. 3e derived from QuikSCAT are different from the ones in Fig. 2b derived from the observation data of Shanghai Typhoon Institute. Since the spatial resolution of QuikSCAT (1°×1°) is low, and the data are averaged for 3 days, the 10-m winds in QuikSCAT are much weaker than the simulated. The absence of observation at high temporal and spatial resolutions is the main challenge in the investigation of air-sea interaction during a typhoon event. We therefore have to rely on numerical simulations to study the mechanisms of air-sea interaction during Typhoon Kaemi.

4. The mechanisms of air-sea interaction

4.1 Thermodynamic factors

The SST cooling is mainly induced by entrainment mixing, upwelling, and wind-current resonance, all of which are the ocean response to typhoon forcing (Tsai et al., 2008). Price (1981) pointed out that typhoons with strong winds could induce SST cooling due to strong disturbances associated with entrainment mixing and upwelling. Contrary to CTRL with the fixed SST, the region of the lowest SST in COUP is near the typhoon center at 42 h (17.02°N, 130.43°E) (Fig. 3d) and due to the time lag of the ocean response, the SST at this moment is just 1°C lower than surrounding water and does not reach its lowest value during the simulation period. As shown in Fig. 2b, the maximum wind speed is 39 m s^{-1} at 42 h. This is consistent with the maximum SST cooling rate of more than 3°C, located to the left of the typhoon track (16.25°N, 130.1°E) in Fig. 4.

The upper ocean cooling induced by TCs in open ocean has attracted significant attention of the researchers. The most striking feature of this cooling is the biased pattern caused by the high correlation between the wind and ocean current on the right side of the storm track in the Northern Hemisphere (Tsai et al., 2008). In terms of SST cooling preference relative to typhoon track (Fig. 3a), there is markedly rightward shift of the ocean response as revealed through three-dimensional coupled model simulations (Bender et al., 1993; Falkovich et al., 1995; Bender and Ginis, 2000; Chan et al., 2001). The shift is associated with the entrainment, which is parameterized as a function of wind stress, velocity shear at the base of ML, and convective overturning due to the surface buoyancy flux in the vicinity of typhoon center (Wu et al., 2005). Plenty of observations and simulations found that the maximum SST cooling occurred to the right or near or on typhoon track (Fisher, 1958; Leipper, 1967; Price, 1981; Black, 1983; Greatbatch, 1985; Stramma et al., 1986; Shay et al., 1992; Suetsugu et al., 2000; Bender and Ginis, 2000; Sadhuram, 2004; Ren et al., 2004). On the other hand, the irregular cooling patterns are produced near the continental shelf area because the regional geometry and bathymetry interact with the storm-induced circulation. Mitchell et al. (2005), for example, found that the greater vertical mixing generated to the right of storm track hindered the development of the bottom Ekman layer and weakened the onshore flows of the cooler off-shelf water, resulting in stronger cooling on the left side of track. Here, we focus on the causes of SST cooling and take two points situated to the left (16.25°N, 130.1°E; point A) and right (17.79°N, 130.46°E; point B) of the typhoon track, respectively, as sampling locations (Fig. 4).

The MLD is closely related to the development of TC, and meanwhile, the strong winds associated with TC can affect the MLD due to ocean water mixing and entrainment. In the present study, the definition of MLD is related to the temperature lapse rate where the SST biases are no less than 0.5°C (Levitus, 1982). The upwelling of colder water to surface can decrease the temperature of ML and cause deepening of the MLD. As shown in Fig. 5, there is a dramatic MLD deepening along the typhoon track and the maximum deepening reaches 50–60 m at 42 h. The anomalies of MLD between COUP and PTRL at point A are 10 m

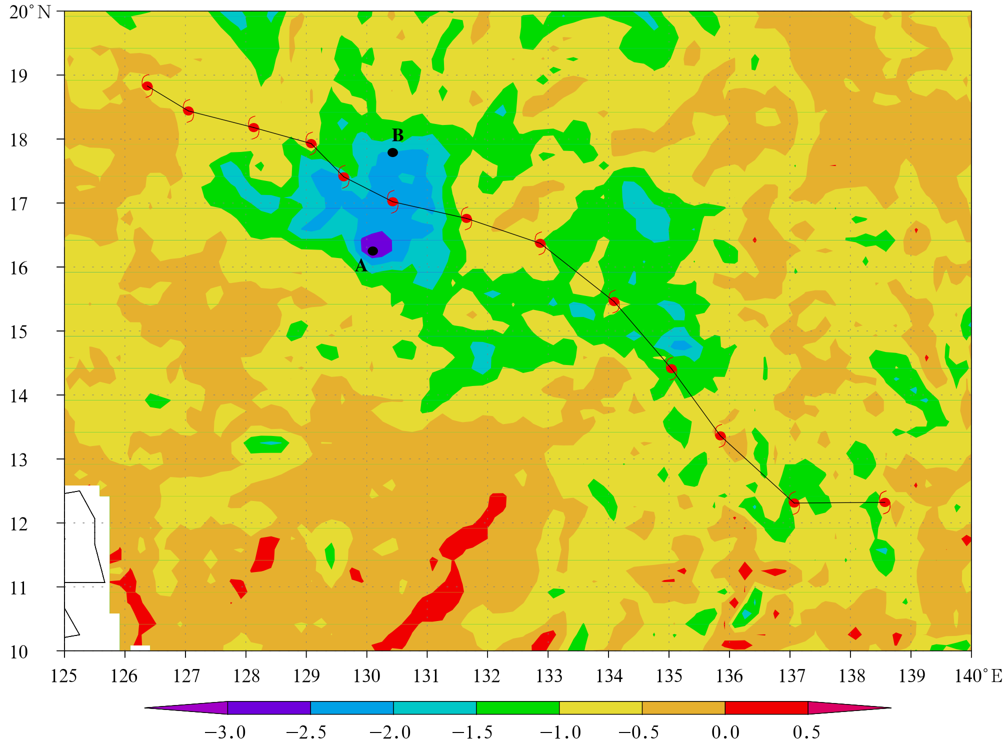

Fig. 4. Typhoon track in COUP and the anomalies of SST (°C; COUP minus PTRL) at 42 h (● is the sampling point).

deeper than at point B, which is consistent with the maximum SST cooling. At 72 h (Fig. 5b), the MLD deepening is still continuing, and the maximum anomalies are 60–80 m along the typhoon track, which indicates that the upper ocean response lasts more than 72 h.

Figure 6 shows the time evolution of temperature at points A (Fig. 6a) and B (Fig. 6b). At the initial time, the temperature of ML at point A is colder than B and the MLD is shallower. From 0000 UTC 21 July, the colder water under thermocline is pumped upward and the SST begins to drop at 1200 UTC 21 July. While at point B, there is no dramatic colder water ascending under thermocline at this moment. At 1800 UTC 21 July (42 h of the simulation), the temperature at point A falls quickly and reaches its minimum of ∼26.4°C. In Fig. 7, the 10-m wind speed at points A and B shares a similar magnitude before 1800 UTC 21 July and both reach the peaks from 1800 UTC 21 to 0600 UTC 22 July, while the winds at point A are relatively stronger than at point B. The lowest temperature at point A is consistent with the pattern of the 10-m winds. Hereafter, the temperature rises gradually and reaches its peak at 1200 UTC 22 July. At point B, when the strongest 10-m winds occur around 42 h of the simulation, there is no extreme low temperature. Afterwards, the temperature decreases gradually and reaches its lowest at 1800 UTC 22 July.

There is no good consistency between the temperature and the 10-m winds at point B. The main cause for the deeper SST cooling at point B probably results from the wind-current resonance (Tsai et al., 2008). It is known that the resonant ocean response occurs as the wind fluctuation approaches the inertial frequency. The internal waves are observed at both points A and B at 42 h during the passage of typhoon Kaemi, as seen from a large vertical displacement of the thermocline simulated by the coupled model (Fig. 7a). The time series of water temperature profiles at the depth of 50 m at points A and B are characterized by the near-inertial oscillations, with a period of 41 h, which is in agreement with the theoretical value at 16.25° and 17.79°N (Wu et al., 2008; Tsai et al., 2008; Chen et al., 2010). However, the oscillations at point

B are much stronger than at point A and the temperature difference between the peak and valley at point B is larger. All of above indicates that the mechanism of the temperature dropping at point A is different from B. The former is more sensitive to the upwelling induced by Ekman pumping. At point B, the

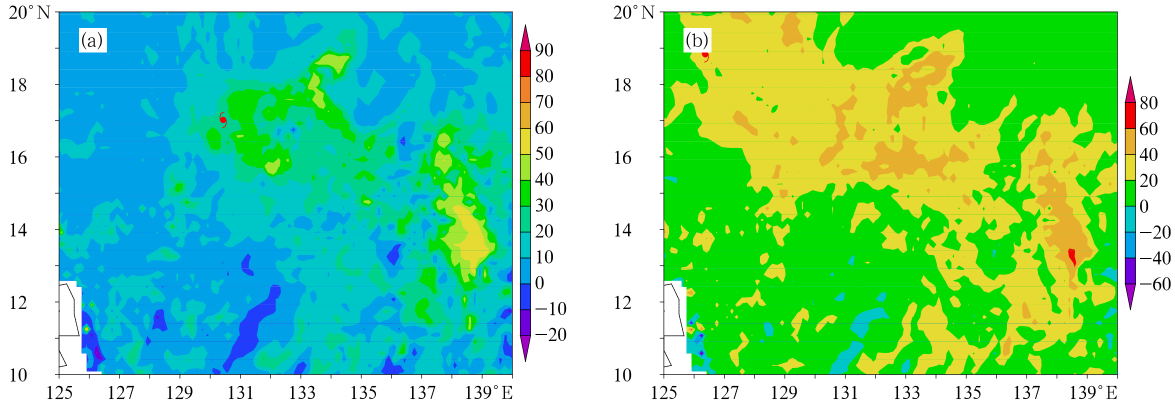

Fig. 5. Anomalies of MLD (m) between COUP and PTRL at (a) 42 h and (b) 72 h (typhoon symbol is used to denote the typhoon center).

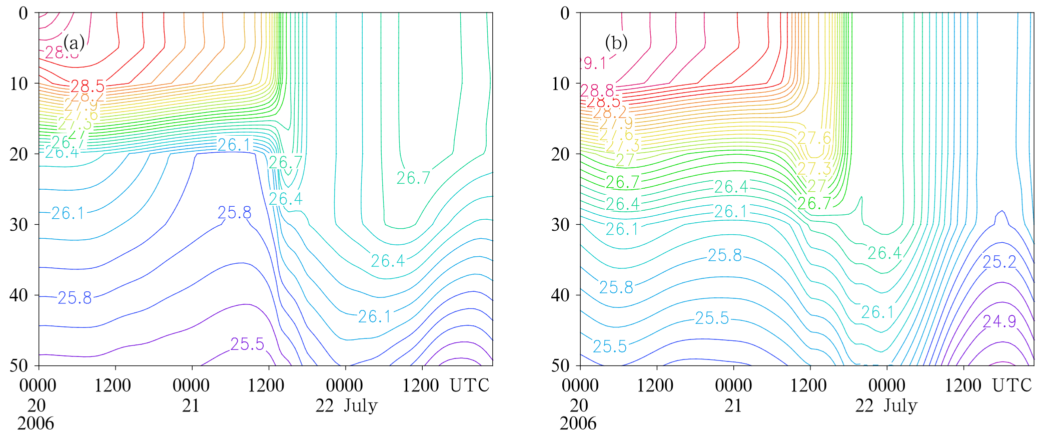

Fig. 6. Time series of temperature (°C) at (a) point A and (b) point B.

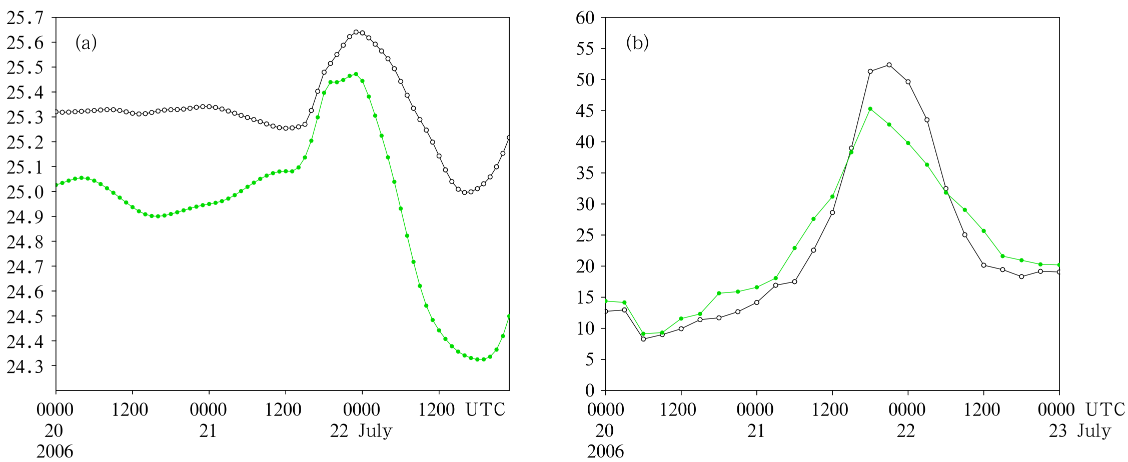

Fig. 7. (a) Time series of temperature profiles (°C) at point A (○) and point B (•) at the depth of 50 m; (b) time series of 10-m wind profiles (m s^{-1}) at point A (○) and point B (•).

oscillations induced by the wind-current resonance are the main reason for the temperature change.

4.2 Dynamic factors

Price et al. (1994) indicated that the ocean cooling induced by upwelling could be evaluated through the nondimensional parameters—the Rossby number Q, which is related to the upwelling length. Figure 8 shows that the relative high Rossby number in COUP at 42 h is to the left rear of the typhoon center, corresponding to the strong 10-m winds at point A. The typhoon winds cause the cyclonic rotation and the vertical entrainment of deep colder water, bringing it upward to the upper ocean. For such events, the vertical entrainment is of great importance to the subsequent motions and cooling in the upper ocean. Momentum budget analysis is performed to identify the process responsible for the vertical entrainment. Figure 9 shows the temporal variations of the vertical diffusion in the momentum equation. In comparison, point A shows stronger and deeper vertical momentum variations than point B. The vertical diffusivity at point A reaches 85 m and is about 10 m deeper than at point B. Thus, the winds causing entrainment pump deeper

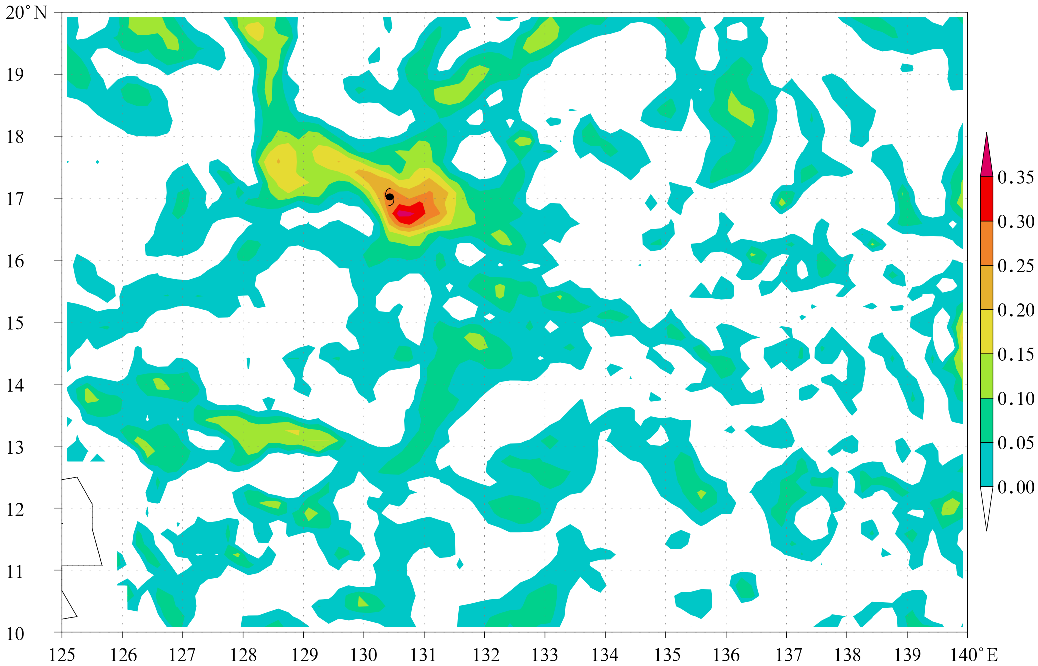

Fig. 8. Rossby number at 42 h (COUP minus PTRL).

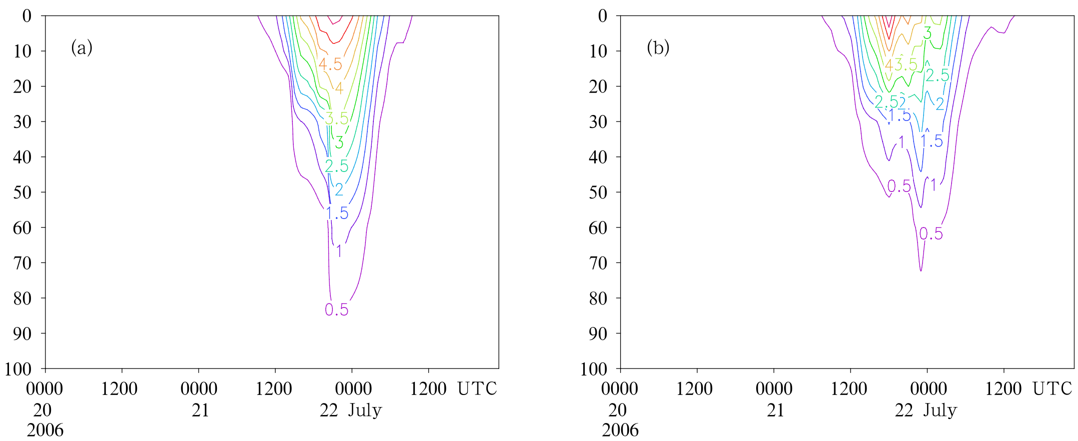

Fig. 9. Time series of vertical diffusivity profiles ($m^2\ s^{-1}$) at (a) point A and (b) point B.

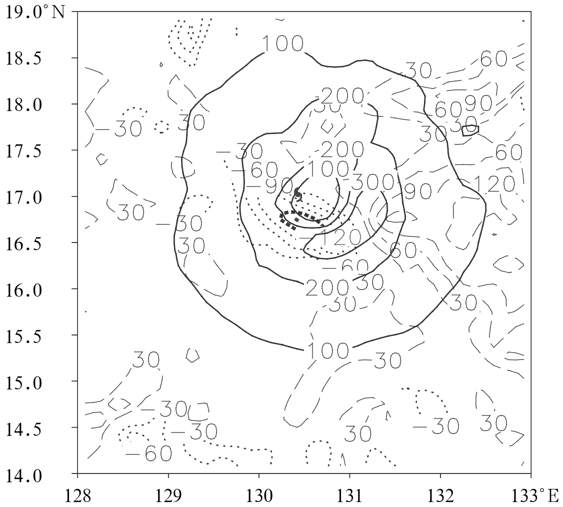

Fig. 10. Wind stress curl (solid line; unit: $10^4\times$dyne cm^{-3}) and current divergence (long dashed line is positive whereas dotted line is negative; unit: 10^2 s^{-1}) in COUP.

and colder water to cause the SST cooling.

The major factor in generating a strong and persistent wake is the wind-current resonance. It is known that the resonant ocean response occurs as the wind fluctuation approaches the inertial frequency. The coupling is particularly good in the rear right quarter of a typhoon because in this region a ocean current divergence center emerges at a distance from the storm center and the currents are thus turning in the same direction as the wind stress. Figure 10 shows the wind stress curl and current divergence. In COUP, the current divergence center to the right of the typhoon track is close to the typhoon center and is overlapped with a region of strong wind stress, and the currents turn in the same direction as the wind stress. When the wind-current resonance occurs, a significant amount of momentum is transferred downward (Tsai et al., 2008). The intense and persistent inertial pumping is supported by the wind-energy input. Figure 11 plots the time series of horizontal advection and diffusion profiles. The profiles illustrate the importance of horizontal mixing at point B and confirm that the oscillations are the mechanisms of SST cooling. Plueddemann and Farrar (2006) evaluated a slab model performance and found that for strong resonant events, the kinetic energy balance in the slab ML model is unrealistic due to the lack of a damping mechanism to transfer momentum between the ML and the transition layer below.

5. Summary

A high-resolution air-sea coupled model is utilized to investigate the influence of air-sea interaction on Typhoon Keami which originated and developed in northwestern Pacific in July 2006. Three numerical experiments are conducted to reproduce the physical processes. Comparing the observation with two of the numerical experiments, we find that the coupled model can reasonably reproduce the major features of ocean response to the moving TC forcing, including the ocean ML deepening, the SST cooling, and the decay of the typhoon.

In this case, the lowest SST is near the typhoon track and the maximum SST cooling is to the left of

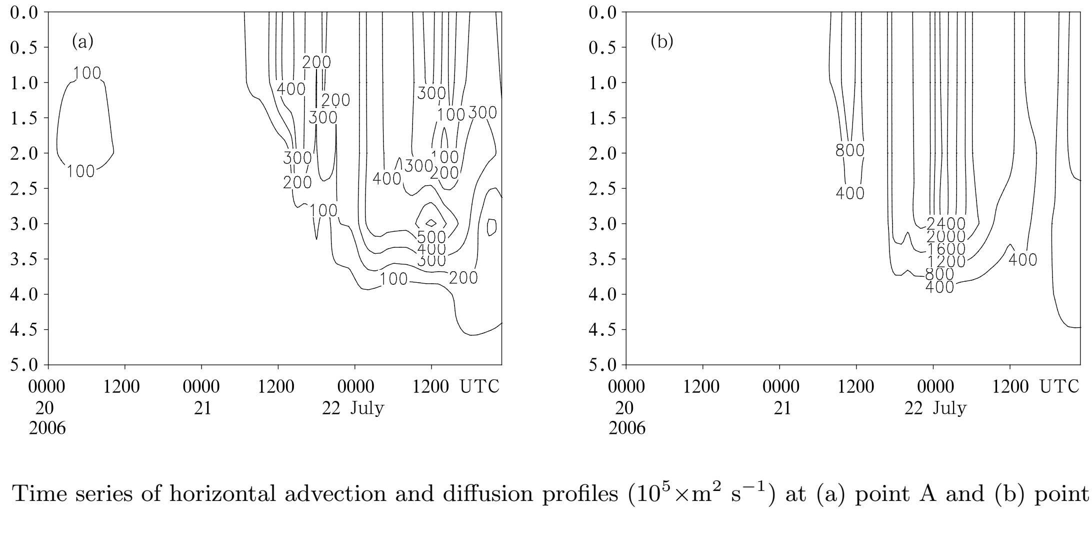

Fig. 11. Time series of horizontal advection and diffusion profiles ($10^5\times$m^2 s^{-1}) at (a) point A and (b) point B.

the track. Two points respectively located to the left (16.25°N, 130.1°E; point A, in the maximum SST cooling region) and right (17.79°N, 130.43°E; point B) of the typhoon track are taken as the sampling points. The thermodynamic and dynamic causes of the SST cooling on the left and right of the typhoon track are analyzed.

At the initial time, the ML at point A is shallower and much colder than that at point B. Since the 10-m winds at point A are stronger at 42 h, the cyclonic rotation induced by Ekman pumping causes entrainment and upwelling. When the typhoon approaches point A, the colder water is pumped upward. The low temperature has a good correlation with the 10-m winds but does not persist a long time, which illustrates that the temperature dropping produced by the entrainment and upwelling is a quick process. Although the wind-current resonance also causes oscillations to the left of the typhoon track, the fluctuation is not so strong as that at point B. The thin ML and upwelling produced by the strong 10-m winds are the main reason that the maximum SST cooling appears to the left of the typhoon track.

Due to the weaker 10-m winds and the thicker and warmer ML at point B, colder water under the thermocline is prohibited and the temperature dropping is not dramatic at the appearance of maximum 10-m winds. For the rest of the simulation time, the temperature gradually decreases, which is caused by the inertial oscillations.

In a word, in the case of Typhoon Keami (2006), the mechanisms of SST cooling are different on the left and right sides of the typhoon track. Such irregular cooling patterns may be produced only in the source region of the North Pacific western boundary current system because the boundary current system and regional geometry and bathymetry interact with the typhoon-induced circulation. Similar phenomenon has been illustrated by Mitchell et al. (2005). Since we simulated only one case, the exact relationship between the SST cooling and the local regional geometry and bathymetry is beyond the scope of this study.

The ocean waves as an important ocean physical phenomenon are not included in the coupled model at present. In the future, we will introduce the waves into the coupled model and identify the local characteristics of ocean response in the source region of the North Pacific western boundary current system.

Acknowledgments. The authors express their thanks to Dr. Ma Chao for providing the ocean data. The QuikSCAT, SODA, AMSR, and TRMM data are downloaded from http://apdrc.soest.hawaii.edu/.

REFERENCES

Bao, J. W., J. M. Wilczak, J. K. Choi, et al., 2000: Numerical simulations of air-sea interaction under high wind conditions using a coupled model: A study of hurricane development. *Mon. Wea. Rev.*, **128**, 2190–2210.

Bender, M. A., I. Ginis, and Y. Kurihara, 1993: Numerical simulations of hurricane-ocean interaction with a high resolution coupled model. *J. Geophys. Res.*, **98**, 23245–23263.

—–, and —–, 2000: Real-case simulations of hurricane-ocean interaction using a high resolution coupled model: Effects on hurricane intensity. *Mon. Wea. Rev.*, **128**, 917–946.

Black, P. G., 1983: Ocean temperature changes induced by tropical cyclones. Ph.D. dissertation, Pennsylvania State University, 278 pp.

—–, E. A. D'Asaro, W. M. Drennan, et al., 2007: Air-Sea exchange in hurricanes: Synthesis of observations from the coupled boundary layer air-sea transfer experiment. *Bull. Amer. Meteor. Soc.*, **88**, 357–374.

Chan, J. C. L., Y. Duan, and L. K. Shay, 2001: Tropical cyclone intensity change from a simple ocean-atmosphere coupled model. *J. Atmos. Sci.*, **58**, 154–172.

Chen, S. S., J. F. Price, W. Zhao, et al., 2007: The CBLAST hurricane program and the next generation fully coupled atmosphere-wave-ocean models for hurricane research and prediction. *Bull. Amer. Meteor. Soc.*, **88**, 311–317.

—–, T. Campbell, H. Jin, et al., 2010: Effect of two-way air-sea coupling in high and low wind speed regimes. *Mon. Wea. Rev.*, **138**, 3579–3602.

Corbosiero, K. L., 2007: Advanced Research WRF high resolution simulations of the inner core structures of Hurricanes Katrina, Rita, and Wilma (2005). Proceedings, 8th Annual WRF Users Workshop, Boulder, CO, NCAR. (http://www.mmm.ucar.edu/wrf/users/workshops/ WS2007/ presentation/2–8_Corbosiero.pdf)

Crawford, G. B., and W. G. Large, 1996: A numerical investigation of resonant inertial response of the ocean to wind forcing. *J. Phys. Oceanogr.*, **26**, 873–891.

Davis, C., W. Wang, S. Chen, et al., 2007: Prediction of landfalling hurricanes with the advanced hurricane WRF model. *Mon. Wea. Rev.*, **136**, 1990–2005.

Emanuel, K. A., 1986: An air-sea interaction theory for tropical cyclones. Part I: Steady-state maintenance. *J. Atmos. Sci.*, **43**, 585–604.

—–, 1988: The maximum intensity of hurricanes. *J. Atmos. Sci.*, **45**, 1143–1155.

Falkovich, A. I., A. P. Khain, and I. Ginis, 1995: Motion and evolution of binary tropical cyclones in a coupled atmosphere-ocean numerical model. *Mon. Wea. Rev.*, **123**, 1345–1363.

Fisher, E. L., 1958: Hurricanes and the sea surface temperature field. *J. Atmos. Sci.*, **15**, 328–333.

Gentry, M. S., 2007: Sensitivity of WRF simulations of Hurricane Ivan to horizontal resolution. M. S. thesis, Dept. of Marine, Earth and Atmospheric Sciences, North Carolina State University, 197 pp.

Gray, W. M., 1998: The formation of tropical cyclones. *Meteor. Atmos. Phys.*, **67**, 37–69.

Greatbatch, R. J., 1985: On the role played by upwelling of water in lowering sea surface temperatures during the passage of a storm. *J. Geophys. Res.*, **90**, 11751–11755.

Holland, G. J., 1997: The maximum potential intensity of tropical cyclones. *J. Atmos. Sci.*, **54**, 2519–2541.

Huang Liwen, Wu Guoxiong, and Yu Rucong, 2005: The effects of mesoscale air-sea interaction heavy rain in two typhoon processes. *Acta Meteor. Sinica*, **63**(4), 455–467. (in Chinese)

Jena, B., M. V. Rao, and B. K. Sahu, 2006: TRMM derived sea surface temperature in the wake of a cyclonic storm over the central Bay of Bengal. *Int. J. Remote Sens.*, **27**(14), 3065–3072.

Kagimoto, T., and T. Yamagata, 1997: Seasonal transport variations of the Kuroshio: An OGCM simulation. *J. Phys. Oceanogr.*, **27**(3), 403–418.

Leipper, D. F., 1967: observed ocean conditions and Hurricane Hilda, 1964. *J. Atmos. Sci.*, **24**, 182–186.

Levitus, S., 1982: Climatological atlas of the world ocean. National Oceanic and Atmospheric Administration Professional Paper, 173 pp.

Lin, I. -I., C. C. Wu, and I. F. Pun, 2008: Upper-ocean thermal structure and the western North Pacific category 5 typhoons. Part I: Ocean features and the category 5 typhoons' intensification. *Mon. Wea. Rev.*, **136**, 3288–3306.

Ma, C., J. Yang, D. Wu, and X. Lin, 2009: The Kuroshio extension: A leading mechanism for the seasonal sea-level variability along the west coast of Japan. *Ocean Dynamics*, **60**, 667–672.

Mellor, G. L., 2004: Users guide for a three-dimensional primitive equation numerical ocean model. Princeton University, Prinveton, NJ 08544–0710, 56 pp.

Mitchell, D. A., W. J. Teague, E. Jarosz, et al., 2005: Observed currents over the outer continental shelf during Hurricane Ivan. *Geophys. Res. Lett.*, **32**, L11610, doi: 10.1029/2005GL023014.

Plueddemann, A. J., and J. T. Farrar, 2006: Observations and models of the energy flux from the wind to mixed-layer inertial currents. *Deep-Sea Res.* II, **53**, 5–30.

Price, J. F., 1981: Upper ocean response to a hurricane. *J. Phys. Oceanogr.*, **11**, 153–175.

—–, T. B. Sanford, and G. Z. Forristall, 1994: Forced stage response to a moving hurricane. *J. Phys. Oceanogr.*, **24**, 233–260.

Raper, S., 1992: Observational data on the relationships between climate change and the frequency and magnitude of severe tropical storms. *Climate and Sea Level Change: Observations Projections and Implications.* R. A. Warrick, E. M. Barrow, and T. M. L. Wigley, Eds., Cambridge University Press, 192–212.

Ren, X. J., P. William, Z. Long, et al., 2004: Atmosphere-Ocean coupled dynamics of cyclones in the midlatitudes. *Mon. Wea. Rev.*, **132**, 2432–2451.

—–, and P. William, 2006: Air-sea interaction of typhoon Sinlaku (2002) simulated by the Canadian MC2 model. *Adv. Atmos. Sci.*, **23**(4), 521–530.

Sadhuram, Y., 2004: Record decrease of sea surface temperature following the passage of a super cyclone over the Bay of Bengal. *Current Science*, **86**, 383–384.

Shay, L. K., P. G. Black, A. J. Mariano, et al., 1992: Upper ocean response to hurricane Gilbert. *J. Geophys. Res.*, **97**, 20227–20248.

Skamarock, W. C., J. B. Klemp, J. Dudhia, et al., 2005: A description of the Advanced Research WRF Version 2. NCAR Tech Notes-468+STR, 88 pp.

Stramma, L., P. Cornillon, and J. F. Price, 1986: Satellite observations of sea surface cooling by hurricanes. *J. Geophys. Res.*, **91**, 5031–5034.

Suetsugu, M., H. Kawamura, and S. Nishihama, 2000: Sea surface cooling caused by typhoons in the western North Pacific Ocean. PORSEC proceedings. Goa, India, **1**, 258–262.

Tsai, Y. L., C. S. Chern, and J. Wang, 2008: The upper ocean response to a moving typhoon. *J. Phys. Oceanogr.*, **64**, 115–130.

Tuleya, R. E., and Y. Kurihara, 1982: A note on the sea surface temperature sensitivity of a numerical model of tropical storm genesis. *Mon. Wea. Rev.*, **110**, 2063–2069.

Wu, C. R., Y. L. Chang, L. Y. Oey, et al., 2008: Air-sea interaction between tropical cyclones Nari and Kuroshio. *Geophys. Res. Lett.*, **35**, L12605, doi:10.1029/2008GL033942.

Wu, L. G., B. Wang, and S. A. Braun, 2005: Impact of air-sea interaction on tropical cyclone track and intensity. *Mon. Wea. Rev.*, **133**, 3299–3314.

Xia, C. S., F. L. Qiao, and Y. Z. Yang, 2006: Three-dimensional structure of the summertime circulation in the Yellow Sea from a wave-tide circulation coupled model. *J. Geophys. Res.*, **111**, C11S03, doi: 10.1029/2005JC003218.

Yin, X. B., Z. Z. Wang, Y. G. Liu, et al., 2007: Ocean response to Typhoon "Ketsana" traveling over the Northwest Pacific and a numerical model approach. *Geophys. Res. Lett.*, **34**, L21606, doi:10.1029/2007GL031477.

Zhu, H. Y., W. Ulrich, and R. Smith, 2004: Ocean effects on tropical cyclone intensification and innercore asymmetries. *J. Atmos. Sci.*, **61**, 1245–1258.